THE JOURNAL OF PHYSICAL CHEMISTRY A
A JOURNAL OF THE AMERICAN CHEMICAL SOCIETY

pubs.acs.org/JPCA

Article

Three-Electron Two-Centered Bond and Single-Electron Transfer Mechanism of Water Splitting via a Copper−Bipyridine Complex

Koteswara Rao Gorantla and Bhabani S. Mallik*

Cite This: *J. Phys. Chem. A* 2023, 127, 160−168

Read Online

ACCESS | Metrics & More | Article Recommendations | Supporting Information

ABSTRACT: We report the atomistic and electronic details of the mechanistic pathway of the oxygen−oxygen bond formation catalyzed by a copper−2,2′-bipyridine complex. Density functional theory-based molecular dynamics simulations and enhanced sampling methods were employed for this study. The thermodynamics and electronic structure of the oxygen−oxygen bond formation are presented in this study by considering the *cis*-bishydroxo, $[Cu^{III}(bpy)(OH)_2]^+$, and *cis*-(hydroxo)oxo, $[Cu^{IV}(bpy)(OH)(=O)]^+$, complexes as active catalysts. In the *cis*-bishydroxo complex, the hydroxide transfer requires a higher kinetic barrier than the proton transfer process. In the case of $[Cu^{IV}(bpy)(OH)(=O)]^+$, the proton transfer requires a higher free energy than the hydroxide one. The peroxide bond formation is thermodynamically favorable for the $[Cu^{IV}(bpy)(OH)(=O)]^+$ complex compared with the other. The hydroxide ion is transferred to one of the Cu−OH moieties, and the proton is transferred to the solvent. The free energy barrier for this migration is higher than that for the former transfer. From the analysis of molecular orbitals, it is found that the electron density is primarily present on the water molecules near the active sites in the highest occupied molecular orbital (HOMO) state and lowest unoccupied molecular orbital (LUMO) of the ligands. Natural bond orbital (NBO) analysis reveals the electron transfer process during the oxygen−oxygen bond formation. The $\sigma^*Cu(d_{xz})-O(p)$ orbitals are involved in the oxygen−oxygen bond formation. During the bond formation, three-electron two-centered ($3e^-$−2C) bonds are observed in $[Cu^{III}(bpy)(OH)_2]^+$ during the transfer of the hydroxide before the formation of the oxygen−oxygen bond.

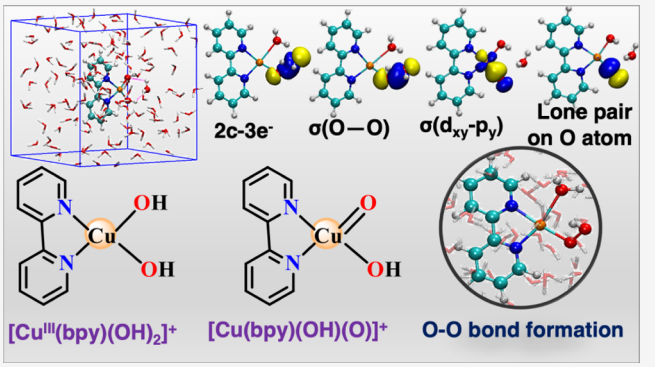

1. INTRODUCTION

Water splitting[1,2] is one of the renewable processes for producing hydrogen fuel, which can be used as an alternative to fossil fuels. The electrons and protons generated during the water oxidation process[3,4] facilitate the hydrogen gas generation,[5,6] and the oxygen−oxygen bond formation is a thermodynamically high energetic process.[7,8] Researchers developed concerned catalysts based on noble and earth-abundant metals to catalyze this process; a blue dimer[9] and water oxidation catalysts (WOCs) based on ruthenium[10,11] and iridium[12,13] metals with good catalytic efficiency were reported. Modifying the ligands[14,15] can effectively decrease the catalytic barrier. Along with iron tetramido macrocyclic ligands,[16] other catalysts with the iron metal[17−20] were reported for water oxidation. Inspired by the oxygen-evolving complex in the photosystem-II, researchers also developed WOCs based on manganese[21−23] and cobalt.[24−27] Moreover, nickel[28−31] and copper[32−34] metal complexes showed promising results. Copper-based metal complexes[35,36] also attracted the researchers' interest due to their high abundance and low cost. Copper metal complexes with different ligands like tetramido,[37] amine−pyridine,[33,38] and tetraaza macrocyclic ligands[39] were reported as WOCs, which were stable under basic conditions. However, the difficulties in accessing the higher oxidation states of the metal complexes lead to higher overpotentials for the water oxidation process. There is a need to find WOCs based on metal−ligand systems, which can lower the overpotentials.

Understanding the mechanistic nature and the structural screening properties will help develop better WOCs based on the first-row transition-metal complexes.[40] The oxygen−oxygen bond formation[41,42] is the most crucial energy-demanding step, which occurs in two pathways. First, the nucleophilic addition of the hydroxide or the water molecule to the metal−oxo complex forms the peroxide complex. Another one is the coupling of the two metal−oxo complexes, which leads to the peroxide intermediate. A few studies[42−44] explored the different ways of oxygen−oxygen bond formation by the

Received: October 31, 2022
Revised: December 15, 2022
Published: January 3, 2023

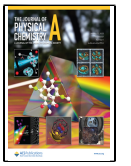

https://doi.org/10.1021/acs.jpca.2c07630
J. Phys. Chem. A 2023, 127, 160−168

oxygen-evolving complex (OEC) in the photosystem-II to understand the mechanistic nature of water oxidation. In most computational studies,[15,45−49] the water molecules' effect on the mechanistic process was studied through implicit solvent models. To get the explicit effect of the water molecules, fully solvated complexes are needed. Molecular dynamics simulations were useful for predicting the solvent water molecules' effect on the water oxidation process[50−54] in an explicit aqueous environment. Moreover, the free energy barriers for the oxygen−oxygen bond formation were reported using the thermodynamic integration method or by applying techniques like metadynamics and blue moon methods.[55] In these processes, the conversion of the reactants to the products happens in the same solvent environment through the formation of the transition states. These molecular dynamics-based studies can help to understand the dynamics of the proton and hydroxide ions involved in the water oxidation process.[56,57]

In the present study, we explore the oxygen−oxygen bond formation by the copper complex with bipyridine ligand[32] in a fully explicit solvated environment. The metal complexes of this ligand with ruthenium,[58,59] iridium,[60,61] and rhodium[62,63] were employed as the catalysts in the small molecules' activation and applications in energy conservation. The free energy landscapes of the water oxidation process were generated with first principles-based well-tempered metadynamics (WT-MetaD) simulations. The oxygen−oxygen bond formation process in the present metadynamics study was explored by defining appropriate collective variables. In the first-row transition-metal complex, the oxygen−oxygen bond formation happens through the nucleophilic addition of the water or hydroxide ion to the metal−oxyl complex. In copper complexes, hydrogen peroxide formation is also possible by reacting the hydroxide with the Cu−OH moiety. In this study, we have investigated the reactivity of the oxygen−oxygen bond formation step by the active catalytic complexes, $[Cu^{III}(bpy)(OH)_2]^+$ and $[Cu^{IV}(bpy)(OH)(=O)]^+$, as given in Figure 1. The electronic orbital structures and kinetic effect of these complexes concerning the water oxidation process are reported in subsequent sections.

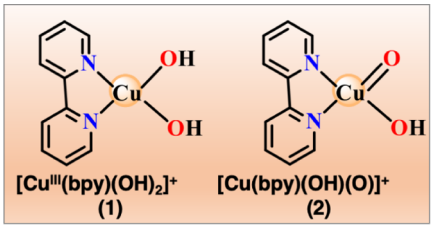

Figure 1. Active catalytic intermediates considered for oxygen−oxygen bond formation.

2. COMPUTATIONAL METHODS

The first-principles molecular dynamics (FPMD) simulations were performed using the CP2K[64] package with a Quickstep[65] module at the Perdew−Burke−Ernzerhof (PBE)[66] exchange−correlation functional with Grimme's D2 dispersion[67] correction. All of the atoms were described by the DZVP-MOLOPT-SR-GTH basis sets[68] along with the GTH-PBE pseudopotentials.[69] The auxiliary plane-wave basis set with 400 Ry cutoff was used. The initial structures for the FPMD simulations were obtained from the classically equilibrated simulations. The details of this method are provided in the Supporting Information. The input geometries for molecular dynamics simulations were obtained from the optimized bishydroxo-2,2′ bipyridine copper complex, $[Cu^{III}(bpy)(OH)_2]^+$ using Gaussian 09[70] at the M06L[71] level with the SDD[72] basis set for copper and 6-31G(d) for other elements. The singlet state was found as the ground state. Analytical frequency calculations were performed at the same level to confirm the minimum structure with no imaginary frequency. The minimum structure for the $[Cu^{IV}(bpy)(OH)(O)]^+$ complex was also determined in the same manner. In this case, the doublet state was the ground spinstate. The FPMD simulations were first performed in the NVT ensemble for 2 ps with an integration step of 0.5 fs to equilibrate the initial geometries obtained from classical molecular dynamics simulations. The average temperature was kept around 300 K with the help of a Nosé−Hoover thermostat.[73,74] The size of the cubic simulation box was determined from the NPT simulations performed for 2 ps at 1 bar pressure and 300 K. The length of the box is 15.81 Å (density = 1.08 gm cm^{-3}) for both the catalytic complexes **1** and **2**. The simulation boxes for the catalytic complexes are shown in Figure S1 of the Supporting Information (SI). Subsequent equilibration for 2 ps at 300 K in the NVT ensemble provided the initial structures for the WT-MetaD simulations.[75,76]

The sampling of free energy profiles for the oxygen−oxygen bond formation by the complexes, shown in Figure 1, was generated through the WT-MetaD method[77] using PLUMED[78] implemented in CP2K. Three independent walkers (for the same metadynamics bias potential) were used to facilitate the sampling of oxygen−oxygen bond formation by all of the complexes. The rigorous error analysis by these three WT-MetaD samplings gives the standard deviation and satisfactory simulation convergence. In WT-MetaD, the bias deposition rate decreases throughout the simulation. The reduction in the bias potential is achieved by rescaling the Gaussian height according to eq 1.

$$\dot{V}(s,t) = \frac{\omega \Delta T \delta_{s,s(t)}}{\Delta T + \omega N(s,t)} = \omega\, e^{-[V(s,t)/\Delta T]}\delta_{s,s(t)} \tag{1}$$

The connection of the above equation with metadynamics is evident by replacing the $\delta_{s,s(t)}$ term with a finite width Gaussian. The height of the Gaussian is determined by

$$w = \omega\, e^{-[V(s,t)/\Delta T]}\tau_G \tag{2}$$

where w is the height of the Gaussian, ω is the initial bias deposition rate, and τ_G is the time interval at which Gaussians were deposited. Finally, the free energy surface (FES) can be estimated as

$$\text{FES}\ \tilde{F}(s,t) = -\frac{T + \Delta T}{\Delta T} V(s,t) \tag{3}$$

The employment of WT-MetaD avoids the risk of overfilling. Another essential thing that influences good FES is the selection of the collective variables (CVs). CVs are the characteristic nature of the coordination number (CN), representing the bond-making and -breaking events (here, the oxygen−oxygen bond formation). These CNs of a specific event can be modulated with proper CVs using the following equation.

https://doi.org/10.1021/acs.jpca.2c07630
J. Phys. Chem. A 2023, 127, 160−168

$$\mathrm{C[A-B]\ or\ CN} = \frac{1-\left(\frac{d_{AB}}{d_0}\right)^p}{1-\left(\frac{d_{AB}}{d_0}\right)^{p+q}} \quad (4)$$

where d_{AB} is the distance between atoms A and B, d_0 is the reference distance, and p and q are the constants. We provided these parameters for each complex in the SI. Initially, Gaussians with a height of 0.3 kcal mol^{-1} were added to the bias potential. The bias factor (γ) of the WT-metaD was appropriately selected to allow the proper sampling of the required barrier. Also, quadratic restraining potentials were employed along with the selected CVs. The restraining (or) wall potentials enables the sampling a limiting space by keeping the water molecule involved in oxygen−oxygen bond formation near the reaction center (metal−hydroxo bond). Apart from these dynamics and free energy calculations, we generated the molecular orbitals in the presence of water molecules to get each reaction state's electronic nature. The natural bond orbital (NBO)[79] analysis was carried out for reactant, product, and transition states involved in the oxygen−oxygen bond formation. We selected these structures without considering the water molecules from metadynamics simulations. Later, generated NBOs for each state at the M06L/cc-pVTZ[80] level to understand the atomic orbitals involved in the reaction and electronic transition during the oxygen−oxygen bond formation by the complexes were studied in this work. The electrophilic nature of the metal−oxo and hydroxo groups was examined by the natural charges. Mulliken and Lowdin spin moments computed along the WT-MetaD also address the electronic and electrophilic nature of intermediates.

3. RESULTS AND DISCUSSION

The *cis*-bishydroxo (**1**) and *cis*-hydroxo(oxo) (**2**) complexes were considered as the active intermediates to examine the oxygen−oxygen bond formation by the copper−bipyridine complexes. These complexes catalyze the water oxidation process in the basic environment. The FES for the oxygen−oxygen bond formed by these complexes was generated using first-principles metadynamics simulations.

3.1. Oxygen−Oxygen Bond Formation by the *cis*-Bishydroxo Copper Complex. The parent complex, $[Cu^{II}(bpy)(OH)_2]$, is converted to $[Cu^{III}(bpy)(OH)_2]^+$(**1**), which is expected to be involved in the oxygen−oxygen bond formation step. Figure 2 shows the solvated structure (1A) of complex **1**, indicating the collective variables (CVs). Two CVs were used to generate the free energy profile for the oxygen−oxygen bond formation. The reaction coordinate of the proton transfers to the cis-hydroxo group is defined along CV1. CV2 represents the coordination number (CN), corresponding to the oxygen−oxygen bond formation between the oxygen atoms of the Cu−O_aH and the water molecule (O_c). CV1 and CV2 keep track of the proton and hydroxide transfer, respectively. Figure 3 shows the FES for the oxygen−oxygen bond formation by complex **1**. The parameters used for the metadynamics simulations are given in Table S1. From 1A, the proton transfers through the transition state 1TS1, and the activation barrier for this proton transfer is 6.6 ± 0.15 kcal mol^{-1}. An intermediate 1I is formed after the proton transfer and stabilized with the free energy of −13.0 ± 0.21 kcal mol^{-1}. Table S2 of SI gives the Mulliken, Lowdin, and natural charges. During the proton migration, a considerable change in spin moments is not observed because of the singlet state. After splitting the water molecule, the hydroxide ion is transferred to the oxygen (O_b) of the intermediate, leading to the formation of the oxygen−oxygen bond. Figure 3 displays the formed intermediates, transition states, and products. The transition state 1TS2 is observed in the hydroxide ion transfer to the Cu−O_b, leading to a peroxide bond. The oxygen−oxygen bond distance in the product state (1B of Figure 3) is 1.76 Å. The activation barrier for the hydroxide transfer is 20.75 ± 0.10 kcal mol^{-1}. The change in free energy for the formation of 1B is −0.96 ± 0.14 kcal mol^{-1}. The proton transfer requires a lower activation barrier than the hydroxide transfer.

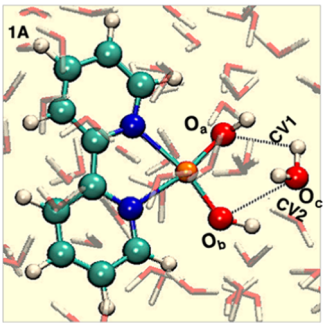

Figure 2. Solvated structure of the $[Cu^{III}(bpy)(OH)_2]^+$ (**1**) indicating the collective variables for the proton and hydroxide transfer for the oxygen−oxygen bond formation.

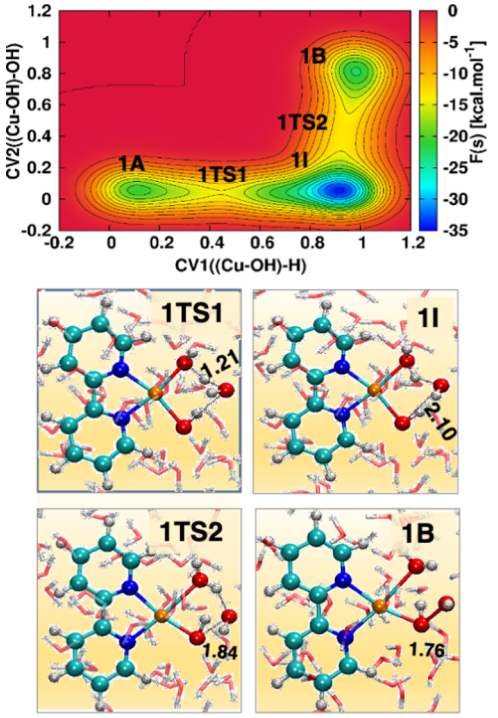

Figure 3. Free energy profile for the oxygen−oxygen bond formation by the *cis*-bishydroxo copper complex. The structures of transition states and other intermediates are also shown.

3.2. Oxygen−Oxygen Bond Formation by the *cis*-Hydroxo(oxo) Copper Complex. This section explores the dynamics of the oxygen−oxygen bond formation by the *cis*-hydroxo(oxo) complex, which is feasible under experimental conditions. Figure 4 shows the solvated structures of the *cis*-hydroxo(oxo) complex and the CVs selected to study the

https://doi.org/10.1021/acs.jpca.2c07630
J. Phys. Chem. A 2023, 127, 160−168

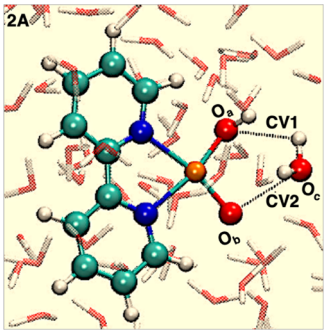

Figure 4. Solvated first minima in the oxygen−oxygen bond formation by the $[Cu^{IV}(bpy)(OH)(=O)]^+$ (**2**) indicating the collective variables for the proton and hydroxide transfer.

oxygen−oxygen bond formation. The water molecule near the reaction center was chosen to model the reaction. CV1 defines the coordination number (CN) of the reaction coordinate for the transfer of the proton to the Cu−O_aH moiety of the complex. The reaction coordinate related to the migration of the hydroxide ion to the Cu−O_b moiety, in forming the oxygen−oxygen bond, was defined with CV2.

Figure 5 shows the FES generated with the help of these CVs for complex 2. The CV parameters applied for the

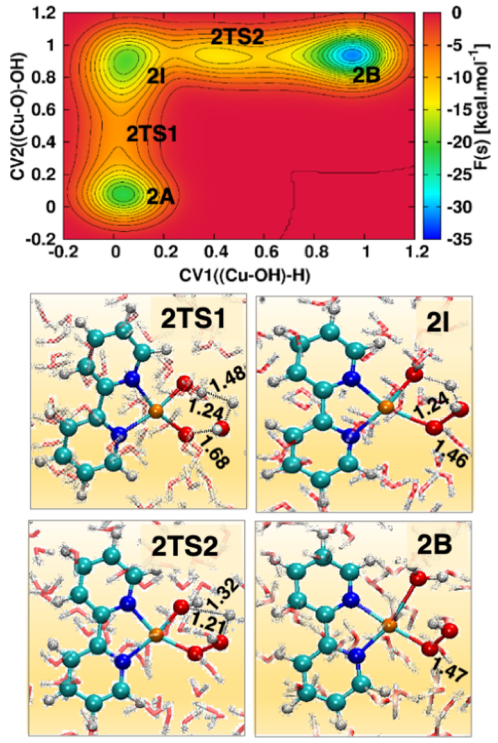

Figure 5. Free energy profile for the oxygen−oxygen bond formation with the structures of transition states and other minima.

metadynamics simulations are tabulated in Table S3. From the solvated minimum structure 2A, the proton and hydroxide ions of the water molecule are transferred to the catalyst's hydroxo and oxo groups. The transition state 2TS1 is observed during the simultaneous migration of the proton and hydroxide ion. Figure 5 displays the intermediates, transition states, and products formed in the oxygen−oxygen bond formation step. The peroxide intermediate 1I is observed after the transfer of the hydroxide to the Cu−O_b moiety. The activation barrier required for the formation of this complex is 9.62 ± 0.44 kcal mol^{-1} through the 2TS1. The formed complex is stabilized with the free energy of 1.8 ± 0.30 kcal mol^{-1}. The proton transfers to the Cu−O_aH group, leading to complex 2B. The activation free energy of migration (14.13 ± 0.53 kcal mol^{-1}) is higher than the hydroxide transfer. The formed complex 2B is stabilized with the free energy of −12.54 ± 0.49 kcal mol^{-1}. The Mulliken and Lowdin spin moments along the natural charges of the atoms involved in the reaction are tabulated in Table S4. The Lowdin spin moment on the oxygen atom O_b is 1.11, indicating the metal−oxygen bond in Cu−$O^{\bullet-}$ rather than the double bond character. The negative Lowdin spin (β-spin is more) moment on the copper helps stabilize complex 2A. The natural charge on the O_c changes from −0.8481 to −0.3338e, indicating the electron density transfer from the water molecule to the catalyst. The Lowdin spin moment of the copper metal changes from −0.04 to 0.65, so a single-electron transfer happens during the nucleophilic addition of the hydroxide ion.[81] The electron density transferred to the catalyst oxidizes the Cu−O_b moiety, further stabilized by the proton's transfer. Therefore, the product state 2B is more stable than intermediate 2I.

Comparing the oxygen−oxygen bond formation by these two complexes, the activation barriers were low for complex 2. These reactions occur in the basic medium; the hydroxide ion dynamics play a crucial role in forming oxygen−oxygen bonds. The free energy for the transfer of hydroxide for all of these complexes is lower than the previously reported first-row metal complexes.[45,48] Figures S2 and S3 represent the variation of the bond distances along with the CVs. The formed oxygen−oxygen (HO_b−O_cH) bond in complex 1 is kinetically less favorable than in complex 2. In the case of complex 2, the migration of hydroxide ion occurs with a lower free energy barrier than complex 1, for which, the hydroxide ion requires higher free energy than the proton transfer. To find the effect of the proton and hydroxide dynamics in the oxygen−oxygen bond formation kinetics, we performed one more simulation with complex 1. The proton from the water molecule is transferred to one of the explicit water molecules instead of the Cu−OH moiety. The hydroxide ion is transferred to the Cu−O_bH moiety. Table S5 represents the parameters of the two CVs. Figure 6 shows the FES generated by using these two CVs along with the minima and TS structures. 1′A of Figure S6 is the solvated structure. The proton is transferred to the oxygen atom (O_d) of the explicit water molecule from this structure. Proton transfer to the explicit water molecule results in an intermediate 1′I (Figure 6), which contains hydronium and hydroxide ions. The transferred hydroxide ion to the Cu−O_bH moiety forms the oxygen−oxygen bond leading to the product state (1′B). The activation free energy values for the proton transfer and hydroxide ion migration are 22.16 ± 0.8 and 24.5 ± 0.8 kcal mol^{-1}, respectively. These values are higher than the first type of mechanisms. The intermediate 1′I is thermodynamically less stable than 1′B. The proton in solution migrates due to other water molecules through the structural diffusion. The migration of the proton and hydroxide ions along the selected CVs is presented in Figure S4. The activation barriers are higher than the earlier mechanism, in which proton transfer occurs to the Cu−OH group. The spin moments and NPA charges of the atoms during the oxygen−oxygen bond formation are tabulated in Table S6 of the SI. The spin moments of the copper and oxygen atoms suggest

https://doi.org/10.1021/acs.jpca.2c07630
J. Phys. Chem. A 2023, 127, 160−168

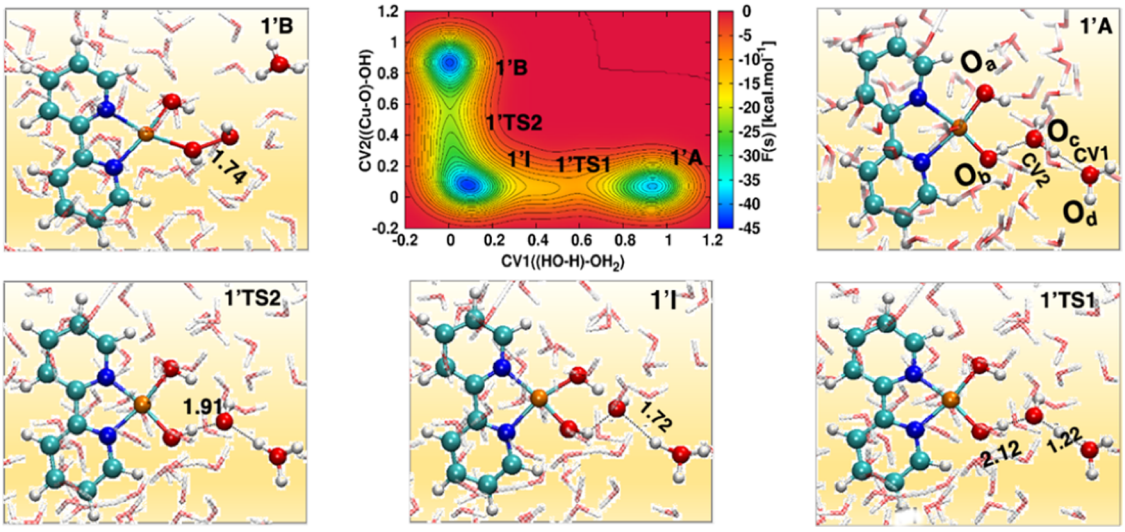

Figure 6. Free energy profile for the oxygen−oxygen bond formation by complex 1 by proton transfer to the explicit water molecule. The structures of transition states and the minima structures are also presented.

that the unpaired electrons on metal and oxygen atoms are in antiparallel spin states. The natural charge on the oxygen atom O_c changes from −1.1262 to −0.7905e. At the same time, the charge on O_b varies from −0.8285 to −0.9552e during the hydroxide ion transfer. These changes indicate that electron transfer happens during the oxygen−oxygen bond. Earlier, a study based on copper−bipyridine reported that the process was termed SET-WNA,[81] where single-electron transfer occurred during the nucleophilic addition of the hydroxide ion. The free energy barrier is little higher in the case of the explicit solvent. The authors computed free energy with different density functional theory methods.

By comparing the dynamics of the hydroxide ion toward the Cu−OH or Cu−$O^{\bullet-}$, it is found that the migration of the hydroxide toward the copper−oxyl group is more favorable than the copper−hydroxo group. Our simulations suggest that the formation of *cis*-Cu−(O−OH)(OH) (2I) is kinetically favored. The formed peroxide complexes, [Cu−(O−OH)-(OH_2)](2B) is more thermodynamically stable than [Cu−(OH−OH)(OH_2)](1B).

3.3. Molecular Orbitals and Electronic Transition during the Oxygen−Oxygen Bond Formation. We computed the highest occupied molecular orbital (HOMO) and lowest unoccupied molecular orbital (LUMO) for the reactant and product states obtained in the above section to find the nature of the electron transfer and properties of the molecular orbitals in the aqueous environment and are shown in Figure 7. The HOMO and LUMO of the product states are given in Figure S5. In the HOMO of 1A, the molecular orbitals are mainly distributed on the water molecules near the Cu−$(OH)_2$ moiety. These water molecules participate in the oxygen−oxygen bond formation through nucleophilic addition. In the LUMO of 1A, the molecular orbital charge is present mainly on the complex but to a lesser extent in the solvent. The HOMO−LUMO gap is 0.70 eV. The HOMO state is the reactive state for the oxygen−oxygen bond formation. The electron density is transferred to the complex in forming the hydrogen peroxide complex (1B). In the HOMO of 1B (Figure S5), the electronic charge is primarily present in the solvent, and a small part is present in the hydrogen peroxide bond. The HOMO of 2A contains the electronic density

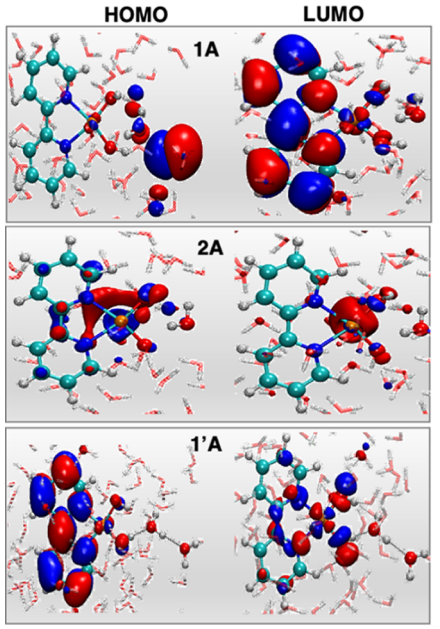

Figure 7. HOMO and LUMO of the reactant states.

mainly on the metal complex. A similar electronic distribution is observed in the case of LUMO. The HOMO−LUMO gap is 0.92 eV. In the HOMO-3 of 2A (Figure S5) state, the water molecules near the reaction center contain more electron density. This state is 1.21 eV lower than the Fermi level. These observations suggest that the water oxidation process proceeds from this state. In 1′A, the electron density is distributed along complex 1 in both HOMO and LUMO cases. The higher electron density on the complex facilitates the proton transfer to the explicit water molecule. The electron density is mainly distributed on the metal center and the peroxide bonds in 1′B, which helps stabilize the Cu−(OOH)(OH) groups. In LUMO, the electron density is present on the formed hydronium ion.

The natural bond orbitals (NBOs) for each state of the reaction were computed to understand the particular orbitals of the complex involved in the oxygen−oxygen bond

https://doi.org/10.1021/acs.jpca.2c07630
J. Phys. Chem. A 2023, 127, 160−168

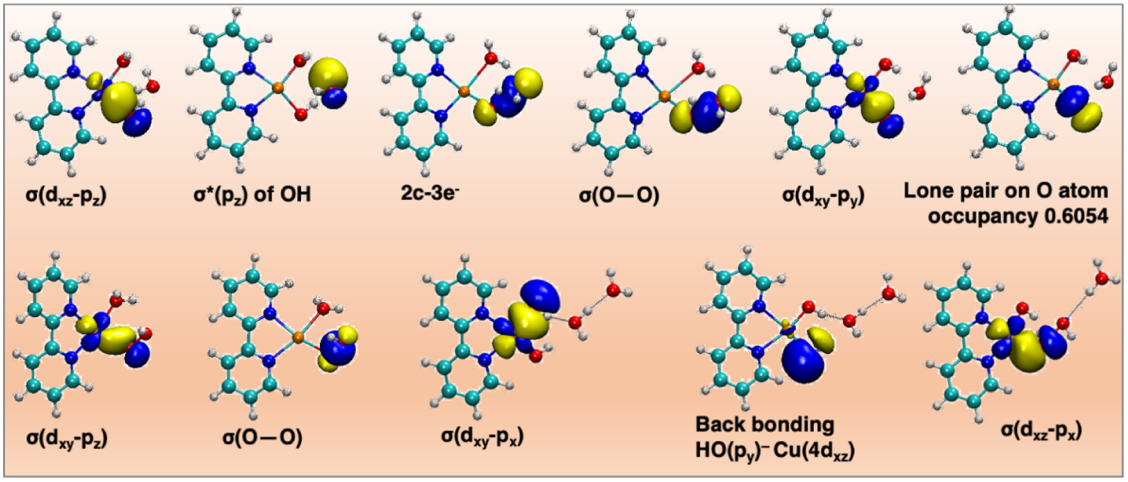

Figure 8. Observed natural bond orbitals (NBOs) during the oxygen−oxygen bond formation. All of the NBOs are drawn with an iso value of 0.04 (for both negative and positive).

formation. Figure 8 represents some of the essential NBOs observed in complexes 1 and 2. These complexes are planar in structure. In complex 1, the d_{xz} and d_{xy} orbitals of the copper metal overlap with the p_z and p_x orbitals of the hydroxide ion's oxygen, forming the σ(Cu−OH) bonds. The σ^*d_{xz}-p_z orbital of the Cu−OH moiety interacts with the σ^*p_z of the OH^- to form the oxygen−oxygen bond. During the migration of the OH^- to the Cu−OH, a three-electron two-centered ($3e^-$−2C) bond is observed at the transition state 1TS2. The $3e^-$−2C bond leads to the formation of the σ(O−O) bond between two hydroxide groups. This bond formation happens through the transfer of a single electron from the hydroxide ion. This type of mechanism is known as SET-WNA, as reported previously.[81] Figure S6 represents some of the other NBOs related to complexes 1 and 2. In the case of complex 2, the Cu−O_b bond is formed by overlapping the d_{xy} orbital of the copper metal with the p_y orbital of the oxygen atom. A lone pair with occupancy of nearly 0.6 is observed on the oxygen atom (O_b). The Cu−O bond distance is 1.79, nearly equal to the Cu−O_aH bond distance. These parameters suggest that the copper−oxo bond has no double bond character, but it is in Cu−$O^{\bullet-}$ nature. The d_{xz} orbital of the copper metal overlaps with the p_x orbital of the oxygen atom (O_aH) from the Cu−O_aH bond. After proton transfer, the hydroxide ion and formed aqua ligand are stabilized by a copper−oxygen bond. The $\sigma^*(d_{xz}$-$p_z)$ of the Cu−O accepting the electron from the p_z orbital of the hydroxide ion forms the oxygen−oxygen bond.

4. CONCLUSIONS

This work explains the mechanistic and electronic details of the oxygen−oxygen bond formation catalyzed by *cis*-bishydroxo $[Cu^{III}(bpy)(OH)_2]^+$ and *cis*-hydroxo(oxo) $[Cu^{IV}(bpy)(OH)(=O)]^+$ copper−bipyridine complexes in this study. The free energy profiles for the oxygen−oxygen bond formation by these complexes were generated through the first-principles metadynamics simulations. The well-tempered metadynamics method was employed to study this process with two collective variables (CVs). The free energy studies reveal that the formation of the oxygen−oxygen bond is favorable for the $[Cu(bpy)(OH)(=O)]^+$. The spin moments change shows the transfer process of the one-electron during the nucleophilic addition of the hydroxide ion. The migration of the hydroxide ion plays an essential role in the formation of the oxygen−oxygen bond. The transfer of the hydroxide ion toward Cu−OH requires a higher activation barrier than the transfer to Cu−$O^{\bullet-}$. In the case of the products, the hydrogen peroxide (Cu−(HO−OH)) is thermodynamically less stable than the peroxide complex (Cu−(O−OH)). In the HOMO state, the electron density is primarily present at the water molecules near the active sites, while in LUMO, the electron density is present on the ligands. The natural charges on the atoms involved in the reaction give evidence for the hydroxide ion's nucleophilic addition to Cu−OH and Cu−$O^{\bullet-}$ bonds. In both complexes, σ^*(Cu(d_{xz})−O(p)) orbitals are involved in the oxygen−oxygen bond formation. In the bis-hydroxo complex, the peroxide bond formation occurs through the formation of the $3e^-$−2C bond, and the single-electron transfer process happens during the nucleophilic addition of the hydroxide ion.

■ ASSOCIATED CONTENT

Supporting Information

The Supporting Information is available free of charge at https://pubs.acs.org/doi/10.1021/acs.jpca.2c07630.

Figures of all simulation box; WT-MetaD parameters and spin moments; NPA charges of the atoms involved in oxygen−oxygen bond formation (PDF)

■ AUTHOR INFORMATION

Corresponding Author

Bhabani S. Mallik − *Department of Chemistry, Indian Institute of Technology Hyderabad, Sangareddy 502284 Telangana, India;* orcid.org/0000-0001-9657-1497; Phone: +914023016285; Email: bhabani@chy.iith.ac.in; Fax: +914023016003

Author

Koteswara Rao Gorantla − *Department of Chemistry, Indian Institute of Technology Hyderabad, Sangareddy 502284 Telangana, India;* orcid.org/0000-0003-4541-8796

Complete contact information is available at: https://pubs.acs.org/10.1021/acs.jpca.2c07630

Notes

The authors declare no competing financial interest.

■ ACKNOWLEDGMENTS

G.K.R. would like to thank UGC, India, for his Ph.D. fellowship.

■ REFERENCES

(1) Barber, J. Photosynthetic Energy Conversion: Natural and Artificial. *Chem. Soc. Rev.* **2009**, *38*, 185−196.
(2) Nocera, D. G. The Artificial Leaf. *Acc. Chem. Res.* **2012**, *45*, 767−776.
(3) Najafpour, M. M.; Moghaddam, A. N.; Allakhverdiev, S. I.; Govindjee. Biological Water Oxidation: Lessons from Nature. *Biochim. Biophys. Acta* **2012**, *1817*, 1110−1121.
(4) Cox, N.; Pantazis, D. A.; Neese, F.; Lubitz, W. Biological Water Oxidation. *Acc. Chem. Res.* **2013**, *46*, 1588−1596.
(5) Maitra, U.; Gupta, U.; De, M.; Datta, R.; Govindaraj, A.; Rao, C. N. R. Highly Effective Visible-Light-Induced H2 Generation by Single-Layer 1T-MoS2 and a Nanocomposite of Few-Layer 2H-MoS2 with Heavily Nitrogenated Graphene. *Angew. Chem., Int. Ed.* **2013**, *52*, 13057−13061.
(6) Amouyal, E. Photochemical Production of Hydrogen and Oxygen from Water: A Review and State of the Art. *Sol. Energy Mater. Sol. Cells* **1995**, *38*, 249−276.
(7) Blakemore, J. D.; Crabtree, R. H.; Brudvig, G. W. Molecular Catalysts for Water Oxidation. *Chem. Rev.* **2015**, *115*, 12974−13005.
(8) Kärkäs, M. D.; Verho, O.; Johnston, E. V.; Åkermark, B. Artificial Photosynthesis: Molecular Systems for Catalytic Water Oxidation. *Chem. Rev.* **2014**, *114*, 11863−12001.
(9) Gersten, S. W.; Samuels, G. J.; Meyer, T. J. Catalytic Oxidation of Water by an Oxo-Bridged Ruthenium Dimer. *J. Am. Chem. Soc.* **1982**, *104*, 4029−4030.
(10) Concepcion, J. J.; Jurss, J. W.; Brennaman, M. K.; Hoertz, P. G.; Patrocinio, A. O. T.; Iha, N. Y. M.; Templeton, J. L.; Meyer, T. J. Making Oxygen with Ruthenium Complexes. *Acc. Chem. Res.* **2009**, *42*, 1954−1965.
(11) Sala, X.; Maji, S.; Bofill, R.; García-Antón, J.; Escriche, L.; Llobet, A. Molecular Water Oxidation Mechanisms Followed by Transition Metals: State of the Art. *Acc. Chem. Res.* **2014**, *47*, 504−516.
(12) Guan, J.; Li, D.; Si, R.; Miao, S.; Zhang, F.; Li, C. Synthesis and Demonstration of Subnanometric Iridium Oxide as Highly Efficient and Robust Water Oxidation Catalyst. *ACS Catal.* **2017**, *7*, 5983−5986.
(13) Brewster, T. P.; Blakemore, J. D.; Schley, N. D.; Incarvito, C. D.; Hazari, N.; Brudvig, G. W.; Crabtree, R. H. An Iridium(IV) Species, [Cp*Ir(NHC)Cl]+, Related to a Water-Oxidation Catalyst. *Organometallics* **2011**, *30*, 965−973.
(14) Vereshchuk, N.; Matheu, R.; Benet-Buchholz, J.; Pipelier, M.; Lebreton, J.; Dubreuil, D.; Tessier, A.; Gimbert-Suriñach, C.; Ertem, M. Z.; Llobet, A. Second Coordination Sphere Effects in an Evolved Ru Complex Based on Highly Adaptable Ligand Results in Rapid Water Oxidation Catalysis. *J. Am. Chem. Soc.* **2020**, *142*, 5068−5077.
(15) Gorantla, K. R.; Mallik, B. S. Understanding the Role of Fluorination in the Mechanistic Nature of the Water Splitting Process Catalyzed by Cobalt Tris-(2-Pyridylmethyl)Amine Complexes. *Sustainable Energy Fuels* **2021**, *5*, 2313−2324.
(16) Ellis, W. C.; McDaniel, N. D.; Bernhard, S.; Collins, T. J. Fast Water Oxidation Using Iron. *J. Am. Chem. Soc.* **2010**, *132*, 10990−10991.
(17) Fillol, J. L.; Codolà, Z.; Garcia-Bosch, I.; Gómez, L.; Pla, J. J.; Costas, M. Efficient Water Oxidation Catalysts Based on Readily Available Iron Coordination Complexes. *Nat. Chem.* **2011**, *3*, 807−813.
(18) Annunziata, A.; Esposito, R.; Gatto, G.; Cucciolito, M. E.; Tuzi, A.; Macchioni, A.; Ruffo, F. Iron(III) Complexes with Cross-Bridged Cyclams: Synthesis and Use in Alcohol and Water Oxidation Catalysis. *Eur. J. Inorg. Chem.* **2018**, *2018*, 3304−3311.
(19) Chen, G.; Chen, L.; Ng, S.-M.; Man, W.-L.; Lau, T.-C. Chemical and Visible-Light-Driven Water Oxidation by Iron Complexes at PH 7−9: Evidence for Dual-Active Intermediates in Iron-Catalyzed Water Oxidation. *Angew. Chem., Int. Ed.* **2013**, *52*, 1789−1791.
(20) Das, B.; Orthaber, A.; Ott, S.; Thapper, A. Iron Pentapyridyl Complexes as Molecular Water Oxidation Catalysts: Strong Influence of a Chloride Ligand and PH in Altering the Mechanism. *ChemSusChem* **2016**, *9*, 1178−1186.
(21) Liao, R.-Z.; Siegbahn, P. E. M. Mechanism for OO Bond Formation in a Biomimetic Tetranuclear Manganese Cluster − A Density Functional Theory Study. *J. Photochem. Photobiol., B* **2015**, *152*, 162−172.
(22) Karlsson, E. A.; Lee, B.-L.; Åkermark, T.; Johnston, E. V.; Kärkäs, M. D.; Sun, J.; Hansson, Ö.; Bäckvall, J.-E.; Åkermark, B. Photosensitized Water Oxidation by Use of a Bioinspired Manganese Catalyst. *Angew. Chem., Int. Ed.* **2011**, *50*, 11715−11718.
(23) Naruta, Y.; Sasayama, M.; Sasaki, T. Oxygen Evolution by Oxidation of Water with Manganese Porphyrin Dimers. *Angew. Chem., Int. Ed. Engl.* **1994**, *33*, 1839−1841.
(24) Dogutan, D. K.; McGuire, R.; Nocera, D. G. Electocatalytic Water Oxidation by Cobalt(III) Hangman β-Octafluoro Corroles. *J. Am. Chem. Soc.* **2011**, *133*, 9178−9180.
(25) Huang, Z.; Luo, Z.; Geletii, Y. V.; Vickers, J. W.; Yin, Q.; Wu, D.; Hou, Y.; Ding, Y.; Song, J.; Musaev, D. G.; Hill, C. L.; Lian, T. Efficient Light-Driven Carbon-Free Cobalt-Based Molecular Catalyst for Water Oxidation. *J. Am. Chem. Soc.* **2011**, *133*, 2068−2071.
(26) McGuire Jr, R.; Dogutan, D. K.; Teets, T. S.; Suntivich, J.; Shao-Horn, Y.; Nocera, D. G. Oxygen Reduction Reactivity of Cobalt(II) Hangman Porphyrins. *Chem. Sci.* **2010**, *1*, 411−414.
(27) Lei, H.; Han, A.; Li, F.; Zhang, M.; Han, Y.; Du, P.; Lai, W.; Cao, R. Electrochemical, Spectroscopic and Theoretical Studies of a Simple Bifunctional Cobalt Corrole Catalyst for Oxygen Evolution and Hydrogen Production. *Phys. Chem. Chem. Phys.* **2014**, *16*, 1883−1893.
(28) Feizi, H.; Bagheri, R.; Jagličić, Z.; Singh, J. P.; Chae, K. H.; Song, Z.; Najafpour, M. M. A Nickel(II) Complex under Water-Oxidation Reaction: What Is the True Catalyst? *Dalton Trans.* **2019**, *48*, 547−557.
(29) Lin, J.; Kang, P.; Liang, X.; Ma, B.; Ding, Y. Homogeneous Electrocatalytic Water Oxidation Catalyzed by a Mononuclear Nickel Complex. *Electrochim. Acta* **2017**, *258*, 353−359.
(30) Wang, L.; Duan, L.; Ambre, R. B.; Daniel, Q.; Chen, H.; Sun, J.; Das, B.; Thapper, A.; Uhlig, J.; Dinér, P.; Sun, L. A Nickel (II) PY5 Complex as an Electrocatalyst for Water Oxidation. *J. Catal.* **2016**, *335*, 72−78.
(31) Wang, D.; Bruner, C. O. Catalytic Water Oxidation by a Bio-Inspired Nickel Complex with a Redox-Active Ligand. *Inorg. Chem.* **2017**, *56*, 13638−13641.
(32) Barnett, S. M.; Goldberg, K. I.; Mayer, J. M. A Soluble Copper−Bipyridine Water-Oxidation Electrocatalyst. *Nat. Chem.* **2012**, *4*, 498−502.
(33) Coggins, M. K.; Zhang, M.-T.; Chen, Z.; Song, N.; Meyer, T. J. Single-Site Copper(II) Water Oxidation Electrocatalysis: Rate Enhancements with $HPO_4$2− as a Proton Acceptor at PH 8. *Angew. Chem., Int. Ed.* **2014**, *53*, 12226−12230.
(34) Nestke, S.; Ronge, E.; Siewert, I. Electrochemical Water Oxidation Using a Copper Complex. *Dalton Trans.* **2018**, *47*, 10737−10741.
(35) Zhang, M.-T.; Chen, Z.; Kang, P.; Meyer, T. J. Electrocatalytic Water Oxidation with a Copper(II) Polypeptide Complex. *J. Am. Chem. Soc.* **2013**, *135*, 2048−2051.
(36) Xiang, R.-J.; Wang, H.-Y.; Xin, Z.-J.; Li, C.-B.; Lu, Y.-X.; Gao, X.-W.; Sun, H.-M.; Cao, R. A Water-Soluble Copper−Polypyridine Complex as a Homogeneous Catalyst for Both Photo-Induced and Electrocatalytic O2 Evolution. *Chem. - Eur. J.* **2016**, *22*, 1602−1607.
(37) Garrido-Barros, P.; Funes-Ardoiz, I.; Drouet, S.; Benet-Buchholz, J.; Maseras, F.; Llobet, A. Redox Non-Innocent Ligand Controls Water Oxidation Overpotential in a New Family of Mononuclear Cu-Based Efficient Catalysts. *J. Am. Chem. Soc.* **2015**, *137*, 6758−6761.

https://doi.org/10.1021/acs.jpca.2c07630
J. Phys. Chem. A 2023, 127, 160−168

(38) Shen, J.; Wang, M.; Zhang, P.; Jiang, J.; Sun, L. Electrocatalytic Water Oxidation by Copper(II) Complexes Containing a Tetra- or Pentadentate Amine-Pyridine Ligand. *Chem. Commun.* **2017**, *53*, 4374−4377.
(39) Yu, F.; Li, F.; Hu, J.; Bai, L.; Zhu, Y.; Sun, L. Electrocatalytic Water Oxidation by a Macrocyclic Cu(II) Complex in Neutral Phosphate Buffer. *Chem. Commun.* **2016**, *52*, 10377−10380.
(40) Kärkäs, M. D.; Åkermark, B. Water Oxidation Using Earth-Abundant Transition Metal Catalysts: Opportunities and Challenges. *Dalton Trans.* **2016**, *45*, 14421−14461.
(41) Siegbahn, P. E. M. Water Oxidation Mechanism in Photosystem II, Including Oxidations, Proton Release Pathways, O-O Bond Formation and O2 Release. *Biochim. Biophys. Acta* **2013**, *1827*, 1003−1019.
(42) Liao, R.-Z.; Siegbahn, P. E. M. Quantum Chemical Modeling of Homogeneous Water Oxidation Catalysis. *ChemSusChem* **2017**, *10*, 4236−4263.
(43) Limburg, J.; Vrettos, J. S.; Liable-Sands, L. M.; Rheingold, A. L.; Crabtree, R. H.; Brudvig, G. W. A Functional Model for O-O Bond Formation by the O2-Evolving Complex in Photosystem II. *Science* **1999**, *283*, 1524−1527.
(44) Kok, B.; Forbush, B.; McGloin, M. Cooperation of Charges in Photosynthetic O2 Evolution-I. A Linear Four Step Mechanism. *Photochem. Photobiol.* **1970**, *11*, 457−475.
(45) Ertem, M. Z.; Cramer, C. J. Quantum Chemical Characterization of the Mechanism of a Supported Cobalt-Based Water Oxidation Catalyst. *Dalton Trans.* **2012**, *41*, 12213−12219.
(46) Ertem, M. Z.; Gagliardi, L.; Cramer, C. J. Quantum Chemical Characterization of the Mechanism of an Iron-Based Water Oxidation Catalyst. *Chem. Sci.* **2012**, *3*, 1293−1299.
(47) Acuña-Parés, F.; Codolà, Z.; Costas, M.; Luis, J. M.; Lloret-Fillol, J. Unraveling the Mechanism of Water Oxidation Catalyzed by Nonheme Iron Complexes. *Chem. - Eur. J.* **2014**, *20*, 5696−5707.
(48) Gorantla, K. R.; Mallik, B. S. Computational Mechanistic Study on Molecular Catalysis of Water Oxidation by Cyclam Ligand-Based Iron Complex. *Theor. Chem. Acc.* **2020**, *139*, No. 161.
(49) Gorantla, K. R.; Mallik, B. S. Mechanism and Dynamics of Formation of Bisoxo Intermediates and O−O Bond in the Catalytic Water Oxidation Process. *J. Phys. Chem. A* **2021**, *125*, 279−290.
(50) Hodel, F. H.; Luber, S. What Influences the Water Oxidation Activity of a Bioinspired Molecular CoII4O4 Cubane? An In-Depth Exploration of Catalytic Pathways. *ACS Catal.* **2016**, *6*, 1505−1517.
(51) Gorantla, K. R.; Mallik, B. S. Iron Complex as a Water-Oxidizing Catalyst: Free-Energy Barriers, Proton-Coupled Electron Transfer, Spin Dynamics, and Role of Water Molecules in the Reaction Mechanism. *J. Phys. Chem. C* **2020**, *124*, 205−218.
(52) Gorantla, K. R.; Mallik, B. S. Mechanism and Electronic Perspective of Oxygen Evolution Reactions Catalyzed by [Fe(OTf)-2(Bpbp)]. *J. Phys. Chem. C* **2021**, *125*, 1313−1322.
(53) Ma, C.; Piccinin, S.; Fabris, S. Reaction Mechanisms of Water Splitting and H2 Evolution by a Ru(II)-Pincer Complex Identified with Ab Initio Metadynamics Simulations. *ACS Catal.* **2012**, *2*, 1500−1506.
(54) de Ruiter, J. M.; de; Buda, F. Introducing a Closed System Approach for the Investigation of Chemical Steps Involving Proton and Electron Transfer; as Illustrated by a Copper-Based Water Oxidation Catalyst. *Phys. Chem. Chem. Phys.* **2017**, *19*, 4208−4215.
(55) Schilling, M.; Cunha, R. A.; Luber, S. Zooming in on the O−O Bond Formation—An Ab Initio Molecular Dynamics Study Applying Enhanced Sampling Techniques. *J. Chem. Theory Comput.* **2020**, *16*, 2436−2449.
(56) Govindarajan, N.; Tiwari, A.; Ensing, B.; Meijer, E. J. Impact of the Ligand Flexibility and Solvent on the O−O Bond Formation Step in a Highly Active Ruthenium Water Oxidation Catalyst. *Inorg. Chem.* **2018**, *57*, 13063−13066.
(57) Wang, Y.; Zhan, S.; Ahlquist, M. S. G. Nucleophilic Attack by OH2 or OH−: A Detailed Investigation on PH-Dependent Performance of a Ru Catalyst. *Organometallics* **2019**, *38*, 1264−1268.
(58) Matheu, R.; Ertem, M. Z.; Benet-Buchholz, J.; Coronado, E.; Batista, V. S.; Sala, X.; Llobet, A. Intramolecular Proton Transfer Boosts Water Oxidation Catalyzed by a Ru Complex. *J. Am. Chem. Soc.* **2015**, *137*, 10786−10795.
(59) Nieto, I.; Livings, M. S.; Sacci, J. B.; Reuther, L. E.; Zeller, M.; Papish, E. T. Transfer Hydrogenation in Water via a Ruthenium Catalyst with OH Groups near the Metal Center on a Bipy Scaffold. *Organometallics* **2011**, *30*, 6339−6342.
(60) DePasquale, J.; Nieto, I.; Reuther, L. E.; Herbst-Gervasoni, C. J.; Paul, J. J.; Mochalin, V.; Zeller, M.; Thomas, C. M.; Addison, A. W.; Papish, E. T. Iridium Dihydroxybipyridine Complexes Show That Ligand Deprotonation Dramatically Speeds Rates of Catalytic Water Oxidation. *Inorg. Chem.* **2013**, *52*, 9175−9183.
(61) Wang, W.-H.; Hull, J. F.; Muckerman, J. T.; Fujita, E.; Himeda, Y. Second-Coordination-Sphere and Electronic Effects Enhance Iridium(III)-Catalyzed Homogeneous Hydrogenation of Carbon Dioxide in Water near Ambient Temperature and Pressure. *Energy Environ. Sci.* **2012**, *5*, 7923−7926.
(62) Conifer, C. M.; Taylor, R. A.; Law, D. J.; Sunley, G. J.; White, A. J. P.; Britovsek, G. J. P. First Metal Complexes of 6,6′-Dihydroxy-2,2′-Bipyridine: From Molecular Wires to Applications in Carbonylation Catalysis. *Dalton Trans.* **2011**, *40*, 1031−1033.
(63) Conifer, C. M.; Law, D. J.; Sunley, G. J.; Haynes, A.; Wells, J. R.; White, A. J. P.; Britovsek, G. J. P. Dicarbonylrhodium(I) Complexes of Bipyridine Ligands with Proximate H-Bonding Substituents and Their Application in Methyl Acetate Carbonylation. *Eur. J. Inorg. Chem.* **2011**, *2011*, 3511−3522.
(64) Hutter, J.; Iannuzzi, M.; Schiffmann, F.; VandeVondele, J. Cp2k: Atomistic Simulations of Condensed Matter Systems. *Wiley Interdiscip. Rev.: Comput. Mol. Sci.* **2014**, *4*, 15−25.
(65) VandeVondele, J.; Krack, M.; Mohamed, F.; Parrinello, M.; Chassaing, T.; Hutter, J. Quickstep: Fast and Accurate Density Functional Calculations Using a Mixed Gaussian and Plane Waves Approach. *Comput. Phys. Commun.* **2005**, *167*, 103−128.
(66) Ernzerhof, M.; Scuseria, G. E. Assessment of the Perdew−Burke−Ernzerhof Exchange-Correlation Functional. *J. Chem. Phys.* **1999**, *110*, 5029−5036.
(67) Grimme, S. Semiempirical GGA-Type Density Functional Constructed with a Long-Range Dispersion Correction. *J. Comput. Chem.* **2006**, *27*, 1787−1799.
(68) VandeVondele, J.; Hutter, J. Gaussian Basis Sets for Accurate Calculations on Molecular Systems in Gas and Condensed Phases. *J. Chem. Phys.* **2007**, *127*, No. 114105.
(69) Goedecker, S.; Teter, M.; Hutter, J. Separable Dual-Space Gaussian Pseudopotentials. *Phys. Rev. B* **1996**, *54*, 1703−1710.
(70) Frisch, M. J.; Trucks, G.; Schlegel, H. B.; Scuseria, G. E.; Robb, M. A.; Cheeseman, J. R.; Scalmani, G.; Barone, V.; Mennucci, B.; Petersson, G. A.; Nakatsuji, H.; Caricato, M.; Xiaosong, L.; Hratchian, H.; Izmaylov, A. F.; Bloino, J.; Zheng, G.; Sonnenberg, J.; Hada, M.; Ehara, M.; Toyota, K.; Fukudaa, R.; Hasegawa, J.; Ishida, M.; Nakajima, T.; Honda, Y.; Kitao, O.; Nakai, H.; Vreven, T.; Montgomery, J. A. J.; Peralta, J. E.; Ogliaro, F.; Bearpark, M.; Heyd, J. J.; Brothers, E.; Kudin, K. N.; Staroverov, V. N.; Keith, T.; Kobayashi, R.; Normand, J.; Raghavachari, K.; Rendell, A.; Burant, J. C.; Iyengar, S. S.; Tomasi, J.; Cosssi, M.; Rega, N.; Millam, J.; Klene, M.; Knox, J.; Cross, J.; Bakken, V.; Adamo, C.; Jaramillo, J.; Gomperts, R.; Stratmann, R.; Yazyev, O.; Austin, A.; Cammi, R.; Pomelli, C.; Ochterski, J.; Martin, R.; Morokuma, K.; Zakrzewski, V.; Voth, G.; Salvador, P.; Dannenberg, J.; Dapprich, S.; Daniels, A.; Farakas, O.; Foresman, J.; Ortiz, J.; Cioslowski, J.; Fox, D. J.*Gaussian 09*, Revision C.01; Gaussian. Inc: Wallingford CT, 2009.
(71) Zhao, Y.; Truhlar, D. G. A New Local Density Functional for Main-Group Thermochemistry, Transition Metal Bonding, Thermochemical Kinetics, and Noncovalent Interactions. *J. Chem. Phys.* **2006**, *125*, No. 194101.
(72) Dolg, M.; Wedig, U.; Stoll, H.; Preuss, H. Energy-adjusted Ab Initio Pseudopotentials for the First Row Transition Elements. *J. Chem. Phys.* **1987**, *86*, 866−872.

https://doi.org/10.1021/acs.jpca.2c07630
J. Phys. Chem. A 2023, 127, 160−168

(73) Nosé, S. A Unified Formulation of the Constant Temperature Molecular Dynamics Methods. *J. Chem. Phys.* **1984**, *81*, 511−519.
(74) Hoover, W. G. Canonical Dynamics: Equilibrium Phase-Space Distributions. *Phys. Rev. A* **1985**, *31*, 1695−1697.
(75) Laio, A.; Parrinello, M. Escaping Free-Energy Minima. *Proc. Natl. Acad. Sci. U.S.A.* **2002**, *99*, 12562−12566.
(76) Laio, A.; Gervasio, F. L. Metadynamics: A Method to Simulate Rare Events and Reconstruct the Free Energy in Biophysics, Chemistry and Material Science. *Rep. Prog. Phys.* **2008**, *71*, No. 126601.
(77) Barducci, A.; Bussi, G.; Parrinello, M. Well-Tempered Metadynamics: A Smoothly Converging and Tunable Free-Energy Method. *Phys. Rev. Lett.* **2008**, *100*, No. 020603.
(78) Tribello, G. A.; Bonomi, M.; Branduardi, D.; Camilloni, C.; Bussi, G. PLUMED 2: New Feathers for an Old Bird. *Comput. Phys. Commun.* **2014**, *185*, 604−613.
(79) Glendening, E. D.; Reed, A. E.; Carpenter, J. E.; Weinhold, F.*NBO*, Version 3.1; TCI University Wisconsin-Madison: Madison, 1998.
(80) Woon, D. E.; Dunning, T. H. Gaussian Basis Sets for Use in Correlated Molecular Calculations. III. The Atoms Aluminum through Argon. *J. Chem. Phys.* **1993**, *98*, 1358−1371.
(81) Funes-Ardoiz, I.; Garrido-Barros, P.; Llobet, A.; Maseras, F. Single Electron Transfer Steps in Water Oxidation Catalysis. Redefining the Mechanistic Scenario. *ACS Catal.* **2017**, *7*, 1712−1719.

https://doi.org/10.1021/acs.jpca.2c07630
J. Phys. Chem. A 2023, 127, 160−168